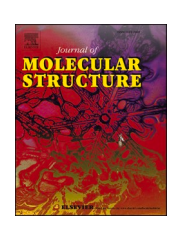
ELSEVIER

Contents lists available at ScienceDirect

# Journal of Molecular Structure

journal homepage: www.elsevier.com/locate/molstr





# Cg...Cg interactions driven 1D polymeric chains bridged by lattice solvents in $N^3$ -(2-pyridoyl)-4-pyridinecarboxamidrazone Pb(II) complex

M.K. Hema <sup>a</sup>, Isabel García-Santos <sup>b,\*</sup>, Alfonso Castiñeiras <sup>b</sup>, Masood Mehrabian <sup>c</sup>, Ennio Zangrando <sup>d</sup>, R. Jyothi Ramalingam <sup>e</sup>, B.N. Ramakrishna <sup>f</sup>, N.K. Lokanath <sup>a</sup>, C.S. Karthik <sup>g,\*</sup>, Ghodrat Mahmoudi <sup>h,\*</sup>

- <sup>a</sup> Department of Studies in Physics, University of Mysore, Manasagangotri, Mysuru 570006, Karnataka, India
- <sup>b</sup> Departamento de Química Inorgánica, Facultad de Farmacia, Universidad de Santiago deCompostela, Santiago de Compostela E-15782, Spain
- <sup>c</sup> Department of Physics, Faculty of Basic Science, University of Maragheh, P.O. Box 55136-553, Maragheh, Iran
- d Department of Chemical and Pharmaceutical Sciences, University of Trieste, Via L. Giorgieri1, Trieste 34127, Italy
- e Department of Chemistry, College of Science, King Saud University, P.O. Box. 2455, Riyadh 11451, Kingdom of Saudi Arabia
- f Department of Physics, Government College for Women (Autonomous), Mandya 571401, Karnataka, India
- <sup>g</sup> Department of Chemistry, SJCE, JSS Science and Technology University, Mysuru 570006, Karnataka, India
- h Department of Chemistry, University of Maragheh, P.O. Box 55181-83111, Maragheh, Iran

#### ARTICLE INFO

# Keywords: Hydrazones Pyridine Pb(II) complex Non-covalent interactions

#### ABSTRACT

This study will shed light on the non-covalent interactions present in the  $N^3$ -(2-pyridoyl)-4-pyridinecarbox-amidrazone Pb(II) complex [(L)Pb(CH<sub>3</sub>OH)(H<sub>2</sub>O)<sub>2</sub>] and their significance in the context of crystal packing and material properties. The complex was synthesized and characterized using single crystal X-ray structural analysis, providing valuable insights into its molecular structure. Our focus was on analyzing the non-covalent interactions in the crystal structure, where these interactions played a crucial role in the formation of one-dimensional network chains observed in the crystal. To quantitatively analyze these interactions, we employed Hirshfeld surfaces analysis. Furthermore, we performed density functional theory computational studies to calculate the molecular geometry and global reactive parameters, allowing us to gain a better understanding of the properties of the novel molecule. The molecular electrostatic potential was plotted to visualize the charge distribution and identify the electrophilic and nucleophilic sites in the molecule. Finally, we explored the non-covalent interactions and electron charge density distribution using the QTAM and NCI models, providing further insights into the complex's behavior. This study contributes to the understanding of non-covalent interactions in the context of crystal growth and design, and expands the knowledge of the structural and electronic properties of the  $N^3$ -(2-pyridoyl)-4-pyridinecarboxamidrazone Pb(II) complex.

## 1. Introduction

Transition metal complexes are renowned for their intriguing properties and diverse reactivities, often exhibiting unique structures and electronic configurations distinct from their parent metal ions [1]. The coordination chemistry of metal complexes with nitrogen-containing ligands has gained considerable attention due to their wide range of applications [2]. Lead, as a heavy metal, has attracted significant interest owing to its toxicological implications and environmental impact [3]. Lead (II) is a well-known transition metal ion known for its versatile coordination chemistry and diverse applications [4].

Pyridinecarboxamidrazones, derived from pyridinecarboxaldehydes or pyridinecarboxamides, hold promise as ligands in coordination chemistry. The presence of a pyridine ring and an amidrazone moiety in these ligands provides multiple coordination sites, facilitating the formation of stable complexes with various metal centers [5]. In recent years, the design and synthesis of transition metal complexes have garnered significant attention due to their potential applications in catalysis, materials science, and medicinal chemistry [6]. Complexes containing heavy metals like lead (Pb) are particularly intriguing due to their distinct electronic structures and reactivity profiles [7].

Designing and synthesizing lead complexes with carefully chosen

E-mail addresses: isabel.garcia@usc.es (I. García-Santos), csk@jssstuniv.in (C.S. Karthik), ghodratmahmoudi@gmail.com (G. Mahmoudi).

<sup>\*</sup> Corresponding authors.

ligands not only contributes to our understanding of the fundamental coordination chemistry of this metal but also opens doors to potential applications [8]. Its ability to form stable complexes with various ligands has made it an attractive choice for scientific and technological advancements [9]. Exploring the coordination behavior of pyridinecarboxamidrazones towards Pb(II) enhances our understanding of fundamental coordination chemistry and offers opportunities for developing functional materials and catalytic systems [10]. Pyridinecarboxamidrazone ligands, with their adjustable electronic and steric properties, show promise in constructing lead complexes with desired properties, such as luminescent materials and catalytic systems [11,12].

Lattice solvents are molecules that occupy the interstitial spaces within the crystal lattice of metal coordination polymers. They can act as ligands or structure-directing agents, influencing the arrangement and properties of the molecular network chains [13]. Solvent-induced transformations of metal complexes are of great interest in applications because they can lead to changes in the structure, properties, and functions of the complexes. For example, solvent-induced transformations can affect the porosity, stability, luminescence, and catalytic activity of metal-organic frameworks (MOFs), which are a class of porous coordination polymers with potential applications in gas storage, separation, sensing, and drug delivery [14,15]. Solvent-induced transformations can also provide insights into the formation and breaking of chemical bonds, the coordination modes and preferences of metal ions and ligands, and the dynamic behavior of metal complexes under different conditions [16,17]. The effect of lattice solvents on the metal coordination environments and the solvent-induced transformations of lead (II) complexes with pyridinecarboxamidrazones are of great interest for understanding the fundamental aspects and practical applications of these systems. Understanding the structural aspects, spectroscopic features, and potential applications of such complexes is crucial for advancing our knowledge of metal coordination chemistry and broadening the practical utilization of these compounds [7]. While the interaction between pyridinecarboxamidrazones and metal ions has been extensively explored for various transition metals such as copper, nickel, cobalt, and zinc [18,19], investigations on the coordination behavior of Pb(II) ions with pyridinecarboxamidrazones are relatively limited.

# 2. Materials and methods

X-ray diffraction analysis: The crystal data for the [(L)Pb(CH<sub>3</sub>OH) (H2O)2] metal complex was collected using Bruker D8 Venture Photon III-14 diffractometer equipped with a low-temperature device, operating at T = 100 K and Mo-K radiation ( $\lambda = 0.71073$  Å) respectively. The data correction for Lorentz-polarization effects and absorption was performed with Bruker APEX3 software [20]. The structure was solved by direct method and refined by full matrix least-squares procedures using the SHELXTL [21]. All the non-hydrogen atoms were refined using anisotropic atomic displacement parameters and hydrogen atoms were inserted at calculated positions using a riding model. Crystal data, data collections, and structural refinement are summarized in-detail and listed in Table 1. Materials for publication were prepared using Diamond 3.2k [22] program and WINGX package (Ver 2018.3) [23]. "CCDC 2267312 contains the supplementary crystallographic data for this paper. These data can be obtained free of charge from The Cambridge Crystallographic Data center via https://www.ccdc.cam.ac.uk/structu res-beta/."

Hirshfeld surface analysis: Intermolecular interactions and surface properties of the molecule in a crystal structure can be well defined by Hirshfeld surface analysis using CrystalExplorer-17.5 software [24]. High resolution molecular hirshfeld surfaces,  $d_{norm}$  and shape index functions were generated for [(L)Pb(CH<sub>3</sub>OH)(H<sub>2</sub>O)<sub>2</sub>] molecule using a crystallographic information file (.CIF file). Hirshfeld surface  $d_{norm}$  mapping defines the distances of any point on the surface to the near est interior

Table 1 Crystal structure data and refinement details of [(L)Pb(CH $_3$ OH) (H $_2$ O) $_2$ ].

| Parameter                               | Value                       |  |  |  |
|---|-----------------------------|--|--|--|
| CCDC deposit no.                        | 2267312                     |  |  |  |
| Empirical formula                       | $C_{25}H_{28}N_{10}O_5Pb_2$ |  |  |  |
| Formula weight                          | 755.76                      |  |  |  |
| Crystal system                          | Monoclinic                  |  |  |  |
| Space group                             | $P2_1/n$                    |  |  |  |
| a (Å)                                   | 12.7238(9)                  |  |  |  |
| b (Å)                                   | 11.0525(7)                  |  |  |  |
| c (Å)                                   | 20.1143(15)                 |  |  |  |
| β (°)                                   | 99.751(2)                   |  |  |  |
| V/(Å <sup>3</sup> )                     | 2787.8(3)                   |  |  |  |
| Z                                       | 4                           |  |  |  |
| D <sub>calcd</sub> (mg/m <sup>3</sup> ) | 1.801                       |  |  |  |
| $\mu  (\text{mm}^{-1})$                 | 6.107                       |  |  |  |
| F(000)                                  | 1480                        |  |  |  |
| $\theta$ range (°)                      | 2.11 - 30.51                |  |  |  |
| Collected reflections                   | 86,013                      |  |  |  |
| Independent reflections                 | 8505                        |  |  |  |
| Rint                                    | 0.0755                      |  |  |  |
| Obs reflections $[I > 2\sigma(I)]$      | 6949                        |  |  |  |
| Parameters                              | 384                         |  |  |  |
| R1 $[I > 2\sigma(I)]$                   | 0.0257                      |  |  |  |
| $wR2 [I > 2\sigma(I)]$                  | 0.0459                      |  |  |  |
| GOF on F <sup>2</sup>                   | 1.018                       |  |  |  |
| Residuals (e Å <sup>-3</sup> )          | 0.942, -0.987               |  |  |  |

 $(d_i)$  and exterior  $(d_e)$  atoms in a molecule. The 2D fingerprint plots were generated by summing  $d_i$  and  $d_e$  obtained from the 3D Hirshfeld surface meanwhile, the percentage contribution of intermolecular interactions was also obtained [25–28].

#### 2.1. Density functional theory

Density functional theory methods were used to calculate the quantum mechanical ground state energy of the molecule and to analyze the electronic structure of the system using *Gaussian 16* software and visualized by GaussView - 6 [29,30]. The electron density function was obtained from an initial approximation of single crystal X-ray diffraction (cif) to compute the electron wave functions. Using the optimized electron density wave function, various physical and chemical properties can be predicted. Koopman's approximation and density of states was used to calculate the energy difference between two molecular orbitals. MEP analysis was carried to determine the electrostatic potential of the molecule. NBO calculation was done to find the hyper conjugative interactions. Furthermore, non-covalent interaction (NCI) and electron charge distribution calculation was done by *multiwfn* 3.7 software [31] and visualized by visual molecular dynamics (VMD 1.9.3) [32].

# 3. Results and discussion

# 3.1. Crystal structure analysis

Through the execution of single crystal structural studies, researchers gain access to precise three-dimensional information, enabling a thorough exploration of non-covalent interactions and bolstering our comprehension of substance properties and behaviors [33–38]. X-ray diffraction analysis revealed that the novel [(L)Pb(CH<sub>3</sub>OH)(H<sub>2</sub>O)<sub>2</sub>] complex is crystallized in monoclinic crystal system with  $P2_1/n$  space group. Mononuclear [(L)Pb(CH<sub>3</sub>OH)(H<sub>2</sub>O)<sub>2</sub>] complex structure is consists of two tridentate  $N^3$ -(2-pyridoyl)-4-pyridinecarboxamidrazone) ligands, two lattice waters and a lattice methanol molecule. *ORTEP* of the title molecule is shown in Fig. 1a.

The ligands in the complex bind to the Pb metal ion through oxygen and nitrogen atoms, creating two chelating rings for each ligand. The way Pb(II) is arranged is described as a distorted trigonal prismatic shape, as shown in Fig. 1b. When we look at the bond distances, we

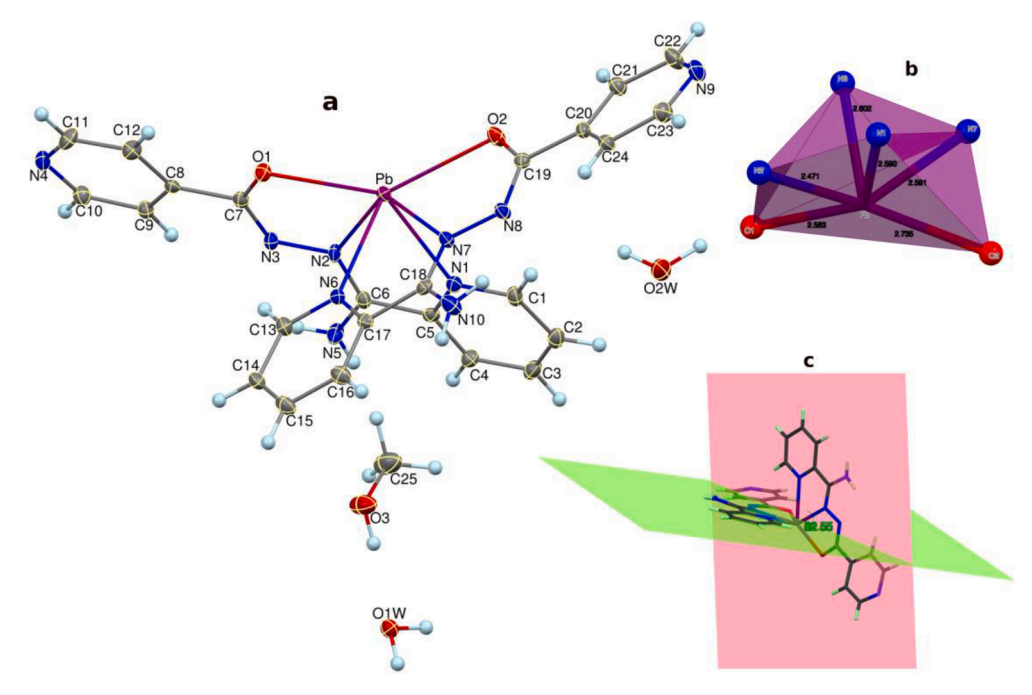


Fig. 1. (a) ORTEP of the novel mononuclear  $[(L)Pb(CH_3OH)(H_2O)_2]$  complex, where thermal ellipsoids drawn at 50% probability, (b) coordination geometry around Pb(II) and (c) interplanar angle between the two coordinated tridentate ligands (non-planarity representation).

notice that the distances between Pb and N/O atoms in the two ligands have slight differences of about 0.10–0.15 Å (Supplementary Table 1). This difference is likely due to specific bonding interactions and structural distortions in the complex. Interestingly, the atoms within both tridentate ligands are almost flat, indicating a high level of planarity in each ligand individually. However, the overall crystal structure of the [(L)Pb(CH<sub>3</sub>OH)(H<sub>2</sub>O)<sub>2</sub>] complex, is remarkably nonplanar concerning the coordinated ligands. This nonplanarity becomes evident from the

interplanar angle between the two tridentate ligands, which measures approximately  $82.55^{\circ}$ , as displayed in Fig. 1c. The nonplanar arrangement of the ligands in the crystal structure may be influenced by various factors, including steric hindrance, interactions between molecules, and other inherent characteristics of the complex [39–41].

The crystal structure of the [(L)Pb(CH<sub>3</sub>OH)(H<sub>2</sub>O)<sub>2</sub>] complex is stabilized by a combination of intra and intermolecular hydrogen bond interactions. Additionally, short ring interactions with Cg–Cg distances

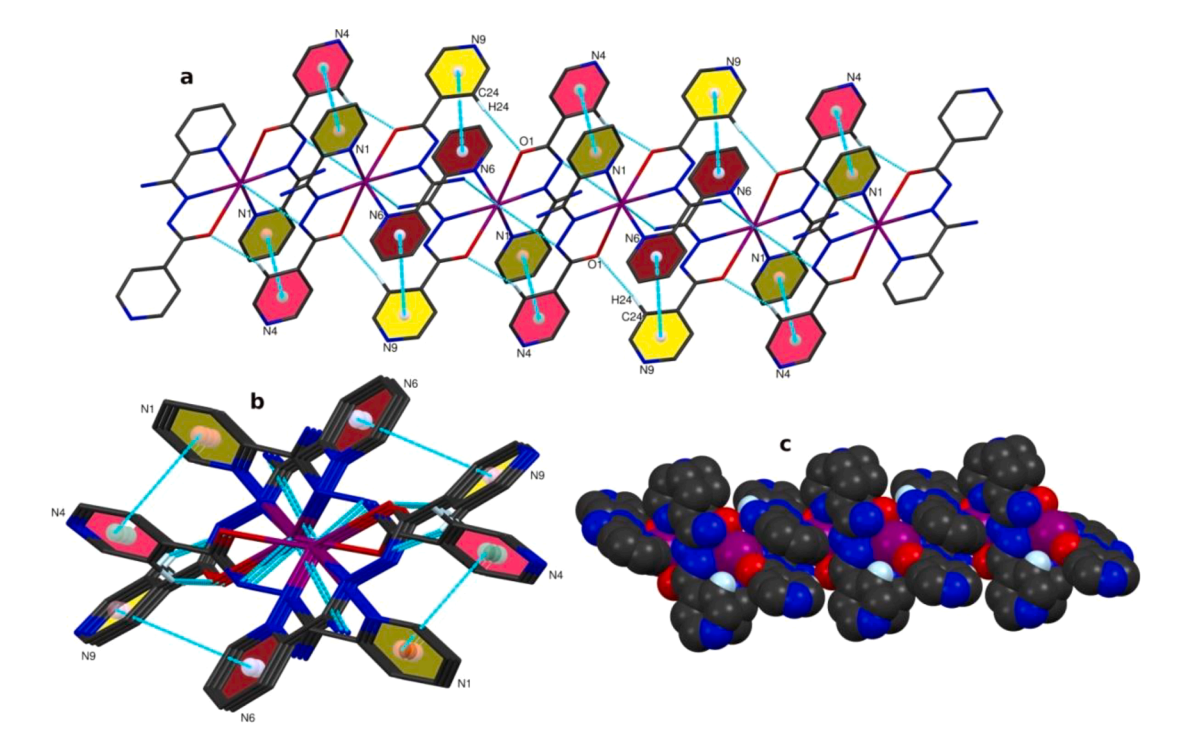
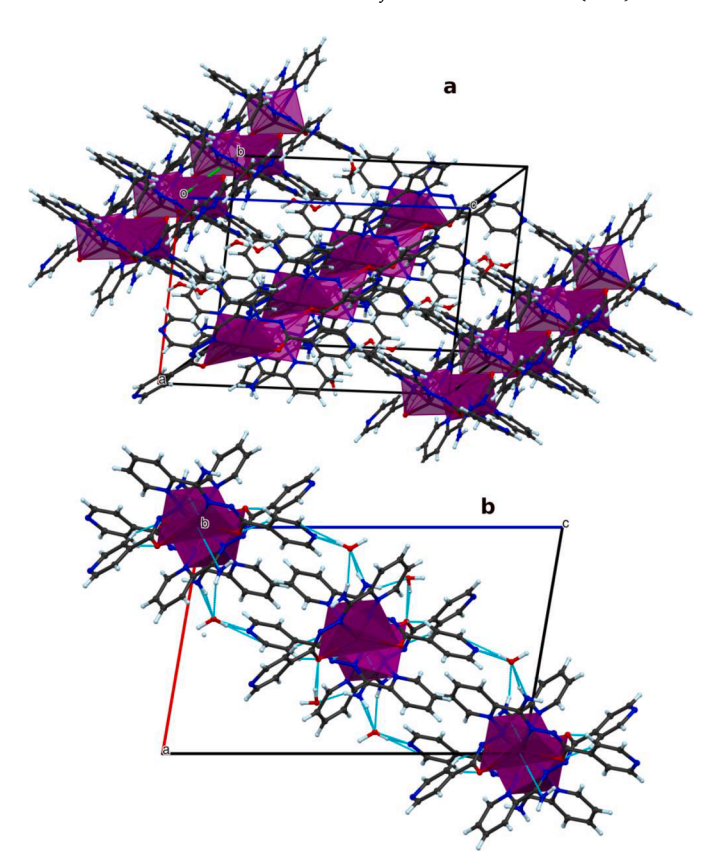


Fig. 2. (a) C24—H24...O1 intermolecular hydrogen bond interaction, Cg...Cg interactions between pyridine rings of neighboring complexes, short interaction between Pb and amine nitrogen of adjacent molecules leading to the 1D network chain; viewed along a-axis. (b) pi...pi stacking when viewed along b-axis and (c) spacefill view of pi..pi stacking along c-axis.

less than 5.0 Å and β angles less than 50.0° contribute to the molecular packing in the crystal [42-44]. One notable interaction is the C24-H24...O1 intermolecular hydrogen bond, which plays a significant role in the crystal packing. Furthermore, there are short interactions between the Pb atom and the amine nitrogen atoms of adjacent molecules, as well as Cg...Cg interactions between the pyridine rings of neighboring complexes, as depicted in Fig. 2a. The crystal structure of the [(L)Pb(CH<sub>3</sub>OH)(H<sub>2</sub>O)<sub>2</sub>] complex reveals the formation of one-dimensional (1D) network chains in the crystal lattice. The formation of these chains is facilitated by several intermolecular interactions, including hydrogen bonding and short ring interactions. Regarding the hydrogen bonds, several potential interactions are observed. For instance, N5-H5a forms a hydrogen bond with O1w, with a hydrogen bond distance (D—H) of 0.82(3) Å and an acceptor distance (H...A) of 2.18(3) Å. Similarly, N5-H5b forms a hydrogen bond with O2w, with D-H of 0.83(4) Å and H...A of 2.06(4) Å. These hydrogen bonds contribute to the stabilization of adjacent molecules within the 1D molecular chains. All four pyridine rings in the molecule are significantly involved in the intermolecular pi...pi stacking (Table 2) with the neighboring molecules forced to the construction of 1D molecular network chains along crystallographic b-axis (Fig. 3a) and these chains are interconnected by lattice waters and methanol (Fig. 3b). In the crystal structure of the [(L)Pb(CH3OH)(H2O)2] complex, both water molecules participate in hydrogen bonding interactions. The involvement of water molecules as double donors and double acceptors in hydrogen bonding interactions has been discussed in the literature. For example, in a study by Desiraju and Steiner, they emphasized the role of water molecules as both donors and acceptors in supramolecular chemistry and crystal engineering. They described the ability of water to form multiple hydrogen bonds and participate in diverse hydrogen bonding patterns in crystal structures [42]. Lattice water molecules acting as double donor and simultaneously as double acceptor with participation of the methanol molecule forming a H-bonding (O-H...O and N—H...O) supramolecular R<sub>4</sub><sup>3</sup>(8) ring motif (Fig. 4a and b). This motif involves hydrogen bonding interactions between adjacent water molecules and other functional groups, connecting multiple adjacent metal complexes within the crystal lattice. Such water-mediated hydrogen bonding networks are crucial for the overall structural organization and stability of the complex in the solid state [44,45].

H···H contacts shown in yellow-colored dotted lines, which involve interactions between hydrogen atoms, play a crucial role in enhancing the stability of the crystal structure (Fig. 5a). The three short bonds observed in this complex, namely H21...H2B: 2.269 (2) Å, H1A...H13:



**Fig. 3.** 1D molecular chains along crystallographic b-axis driven by intermolecular pi...pi stacking between pyridine rings (a) and these chains are interconnected by lattice waters and methanol (b).

2.269 (4) Å, and H4B...H13: 2.033 Å, are formed between the lattice solvents and ligands. These H···H contacts contribute to the overall stabilization of the crystal lattice, promoting a well-defined packing arrangement. Additionally, C...H/H...C contacts are formed between pyridine carbons (C10 and C23) of the tridentate ligand and hydrogens of the lattice water (H3A and H1A). These contacts, represented by green-colored dotted lines, significantly influence the crystal packing by contributing to intermolecular interactions (Fig. 5b). They play a role in determining the arrangement of neighboring molecules and can impact

**Table 2**Hydrogen bond geometry and geometrical parameters for the Pi-stacking moieties involved in the Pi...Pi interactions.

| Potential hydrogen bonds<br>Donor-HAcceptor |             | D–H (Å)            | HA (Å)  | DA (Å)    | D–HA (°) |       | Symmetry                     |             |
|---|-------------|--------------------|---------|-----------|----------|-------|------------------------------|-------------|
| N5—H5aO1w                                   |             | 0.82(3)            | 2.18(3) | 2.902(3)  | 148(3)   |       | 1-x,1-y,-z                   |             |
| N5-H5bO2w                                   |             | 0.83(4)            | 2.06(4) | 2.851(3)  | 159(3)   |       | 1/2-x, $1/2$ + y, $1/2$ -z   |             |
| N10-H10aO2w                                 |             | 0.82(4)            | 2.31(4) | 3.103(3)  | 165(3)   |       | 1/2-x, $-1/2$ + y, $1/2$ -z  |             |
| O3-H13O1w                                   |             | 0.84               | 1.84    | 2.682(3)  | 175      |       | -                            |             |
| O1w-H1aN9                                   |             | 0.92               | 1.84    | 2.752(3)  | 169      |       | 1/2-x, $1/2$ + y, $1/2$ -z   |             |
| O1w—H2bO2                                   |             | 0.86               | 1.85    | 2.690(3)  | 165      |       | 1 + x,y,z                    |             |
| O2w-H2bO3                                   |             | 0.98               | 1.84    | 2.795(3)  | 164      |       | -1/2 + x, 1/2 - y, 1/2 + z   |             |
| O2w-H2aN4                                   |             | 0.92               | 1.85    | 2.757(3)  | 166      |       | -x,1-y,-z                    |             |
| C24—H24O1                                   |             | 0.95               | 2.46    | 3.358(2)  | 155.81   |       | 1/2-x, $1/2 + y$ , $1/2 + z$ |             |
| Short ring-i                                | nteractions |                    |         |           |          |       |                              |             |
| Cg(I)                                       | Cg(J)       | Cg(I)- $Cg(J)$ (Å) |         | α (°)     | β (°)    | γ (°) | Slippage (Å)                 | Symmetry    |
| pyN1  | pyN4        | 3.5858(15          | 5)      | 8.13(12)  | 21.6     | 20.5  | 1.319                        | -x, 1-y, -z |
| pyN4  | pyN1        | 3.5859(15          | 5)      | 8.13(12)  | 20.5     | 21.6  | 1.253                        | -x, 1-y, -z |
| pyN6  | pyN9        | 3.9759(16          | 5)      | 15.01(13) | 27.3     | 29.8  | 1.827                        | -x, -y, -z  |
| pyN9  | pyN6        | 3.9757(16          | 5)      | 15.01(13) | 29.8     | 27.3  | 1.978                        | -x, -y, -z  |

Cg(I) and Cg(J) centroids of the rings, Cg(I)-Cg(J)-Centroid distance between ring I and ring J, Alpha-Dihedral angle between mean planes I and J, Beta-Angle between the centroid vector Cg(I)···Cg(J), the normal to the plane (I), Gamma-Angle between the centroid vector Cg(I)···Cg(J) and the normal to the plane (J), and Slippage-Distance between Cg(I) and Perpendicular Projection of Cg(J) on Ring I (Ang). Where pyN1, pyN4, pyN6 and pyN9 are the centroids of the rings in which nitrogen atom is named as N1, N4, N6 and N9 respectively.

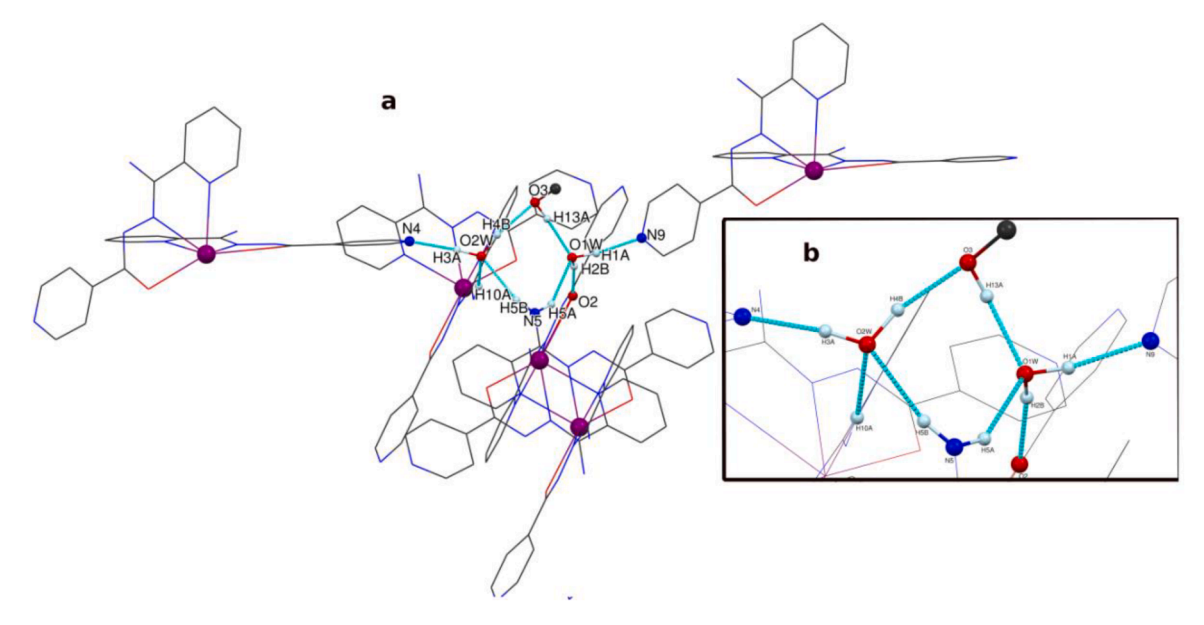


Fig. 4. Lattice water molecules acting as double donor and simultaneously as double acceptor with participation of the methanol molecule forming a H-bonding (O—H...O and N—H...O) supramolecular  $R_4^3(8)$  ring motif (b) by connecting five different adjacent metal complexes (a).

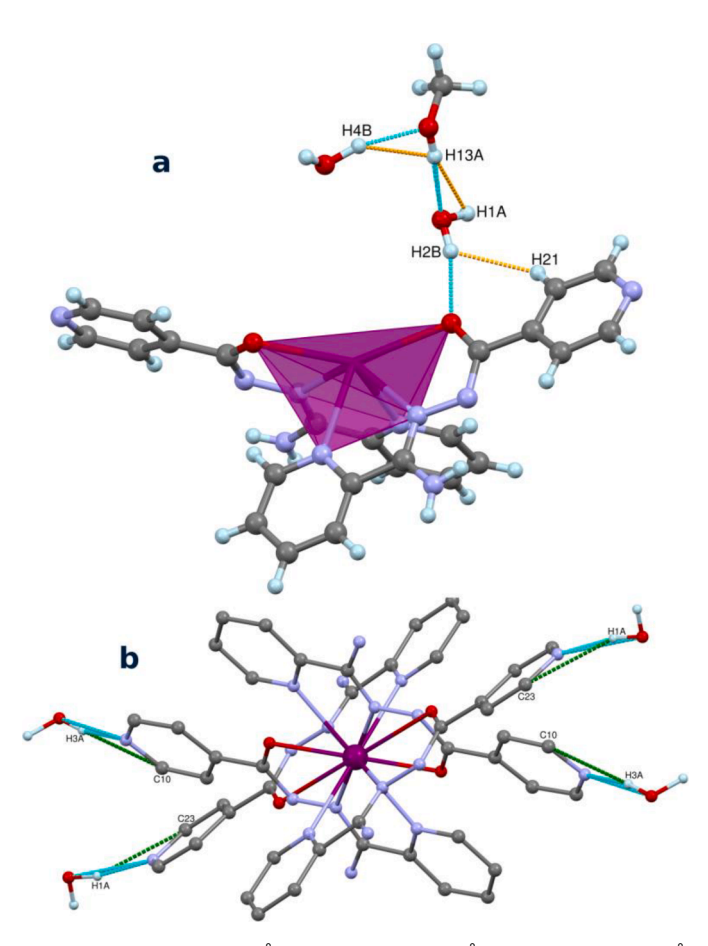


Fig. 5. H21...H2B: 2.269(2) Å, H1A...H13: 2.269(4) Å and H4B...H13: 2.033 Å (yellow colored dotted lines) contacts between lattice solvents and ligand (a) and C...H/H...C contacts (shown in green colored dotted lines) between pyridine carbons (C10 and C23) of tridentate ligand and hydrogens of lattice water [H3A and H1A] (b) are greatly contributed to crystal packing of [(L)Pb(CH $_3$ OH) (H $_2$ O) $_2$ ] complex.

the overall stability and properties of the crystal structure. The presence of these  $H\cdots H$  and  $C\ldots H/H\ldots C$  contacts highlights the intricate interplay between molecular components in the crystal lattice.

#### 3.2. Hirshfeld surface analysis

Hirshfeld surfaces are the effective way to validate the intermolecular interactions in the crystal.  $d_{norm}$  surface and shape idex of [(L)Pb (CH<sub>3</sub>OH)(H<sub>2</sub>O)<sub>2</sub>] complex is generated and shown in Fig. 6. Contacts that are shorter than the total Van der Waals radii of the two atoms are emphasized in red color circular spots on the  $d_{norm}$  surface. Longer contacts are represented by the color blue, while contacts that are close to the Van der Waals limit are colored white.  $d_{norm}$  surfaces in Fig. 6a, b and c, clearly shows that, there are multiple dark red spots which are signifies the intermolecular O—H...O and N—H...O hydrogen bond interactions, whereas in Fig. 6d triangle shaped red colored regions on the pyridine rings indicates significant pi...pi interactions.

The analysis of 2D fingerprint plots revealed that H...H contacts contribute the most to the total Hirshfeld surfaces, accounting for approximately 48.3%. The presence of two distinct peaks at de and di values around 1.12 and 1.14, respectively, signifies the presence of strong hydrogen bonds between water molecules and pyridine nitrogens, lattice methanol, and NH2 amino moiety. These hydrogen bonds are responsible for approximately 15.3% and 10.2% of the total Hirshfeld surfaces, respectively (Fig. 7). The analysis of 2D fingerprint plots reveals that C...H/H...C contacts between pyridine carbons (C10 and C23) of the tridentate ligand and hydrogen atoms of lattice water (H3A and H1A) play a significant role in the crystal packing. These interactions contribute greatly to the total Hirshfeld surfaces, accounting for approximately 11.9% of the surface area. As shown in Fig. 7, 2D fingerprint plots allowed for the quantification of the relative contributions of different intermolecular interactions to the overall Hirshfeld surface.

#### 3.3. Density functional theory studies

The electronic structure of the  $[(L)Pb(CH_3OH)(H_2O)_2]$  complex was analyzed using quantum computational (DFT) studies. The ground state energy optimization was performed in the singlet state using the B3LYP calculation method and the 6-311+G(d,p) basis set. This analysis provides valuable insights into the reactivity, active site selection, and

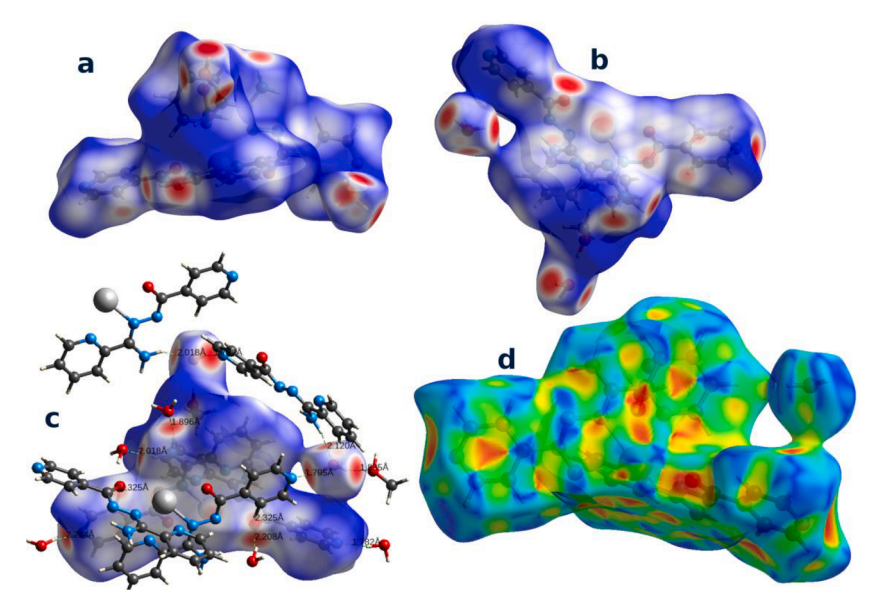


Fig. 6. 3D Hirshfeld surfaces mapped with d<sub>norm</sub>, with different views (a, b and c) and 3D Hirshfeld surface mapped with shape idenx (d) where complimentary blue and red triangles represent pi...pi interactions.

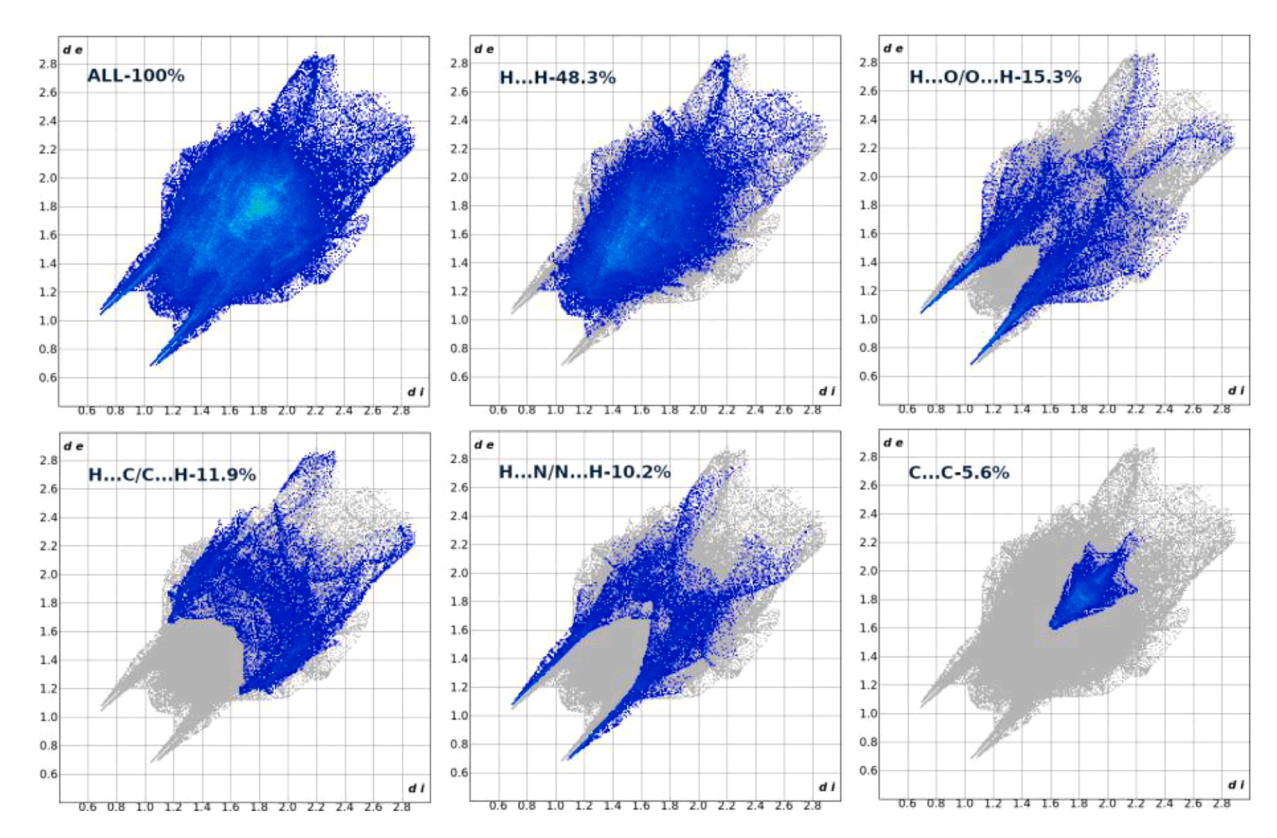


Fig. 7. 2D fingerprint plots and individual atomic contacts% contribution to the total Hirshfeld surface.

stability of the complex. The Pb (II) complex optimized geometries are presented in Fig. 8. It can be evinced from this figure that the calculated geometric features of the structure match very well its counterpart experimentally determined, using X-ray diffraction data. A good correlation was found to exist between the experimental and theoretical structures as is evident from the bond distance table (Table S1).

The configuration and energy values of the Frontier Molecular Orbitals (FMOs) play a crucial role in understanding the chemical and electronic conformation of the complex. The highest occupied molecular

orbital (HOMO) and lowest unoccupied molecular orbital (LUMO) are associated with the ionization potential and electron affinity, respectively. The energy gap between the HOMO and LUMO, which signifies electron excitation, is a key factor influencing the stability and reactivity of the complex. In Fig. 9a, the 3D maps of the HOMO–LUMO show the positive and negative phases represented by violet and yellow colors, respectively. The HOMO is primarily distributed over the Pb metal ion and partially filled with ligands coordinated with the complex above it, while the LUMO is distributed over the Pb metal ion and partially filled

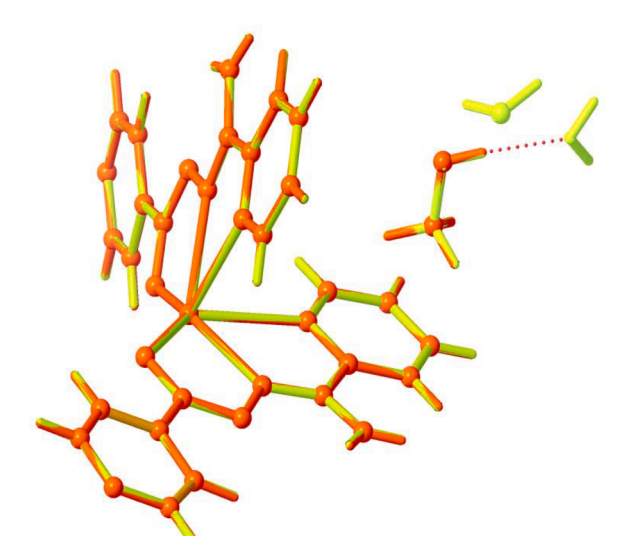


Fig. 8. Overlay of the Optimized structure (orange) and experimentally calculated structure (yellow) of novel complex.

with ligands coordinated with the complex below it.

The global reactivity parameters listed in Table 3, including the global electrophilicity index ( $\omega$ ), global hardness ( $\eta$ ), chemical potential ( $\nu$ ), and global softness (s), provide important insights into the reactivity of the complex. The energy levels of  $E_{HOMO}$  and  $E_{LUMO}$  (–5.6967 eV and –2.5989 eV, respectively) indicate a suitable range for light absorption and emission, suggesting potential applications in photonic and optoelectronic devices. The relatively low energy gap ( $\Delta E$ ) of 3.0978 eV suggests a moderate stability of the complex, which could be advantageous for catalytic reactions. The ionization potential (IP) and electron affinity (EA) values indicate the ability of the complex to both donate and accept electrons, which can be significant for redox processes in catalysis. A soft complex with a low energy gap is generally more reactive and polarizable, which can be beneficial for electrochemical

processes in storage and battery devices. The global electrophilicity index ( $\omega=9.6551$  eV) represents the tendency of the complex to accept electrons. A high electrophilicity index suggests that the complex has a strong potential for participating in redox reactions, which is relevant for energy storage and battery applications. DFT calculated molecular electrostatic potential image of novel complex is shown in Fig. 9b.

#### 3.4. QTAIM and NCI analysis

Bader's theory (QTAIM) has recently been developed as a useful tool for investigating many types of chemical interactions based on electron density topology. Hydrogen bond interactions, ionic and covalent bonding, and relativistic interactions are amongst them. The electron density distribution of a molecule can be used to identify and analyze the strength and nature of intramolecular interactions. The topological AIM analysis displays the existence of BCP 31 (between H13 and O2w) and BCP 25 (between H10a and O2w) confirming the hydrogen bond interactions which are shown in Fig. 10a. Pb(II) complex discloses the presence of the significant hydrogen bond interactions between lattice water and methanol (O3—H13...O2w and N10-H10a...O2w) plays significant repulsions. Weak intramolecular C–H...O interactions between the chelating oxygen atom and -CH group of the phenyl ring and C–H...

Table 3 Global and local parameters of [(L)Pb(CH $_3$ OH)(H $_2$ O) $_2$ ] complex.

| Parameter                                | Molecule value (eV) |  |  |  |
|--|---------------------|--|--|--|
| E <sub>HOMO</sub> (eV)                   | -5.6967             |  |  |  |
| E <sub>LUMO</sub> (eV)                   | -2.5989             |  |  |  |
| Energy gap (ΔE) (eV)                     | 3.0978              |  |  |  |
| Ionization Potential (IP) (eV)           | 4.8961              |  |  |  |
| Electron affinity (EA) (eV)              | 3.1992              |  |  |  |
| Electronegativity (χ) (eV)               | 4.0477<br>0.8485    |  |  |  |
| Global Hardness (η) (eV)                 |                     |  |  |  |
| Softness( $\sigma$ ) (eV <sup>-1</sup> ) | 1.1786              |  |  |  |
| Chemical potential (µ) (eV)              | -4.0477             |  |  |  |
| Global electrophilicity (ω) (eV)         | 9.6551              |  |  |  |

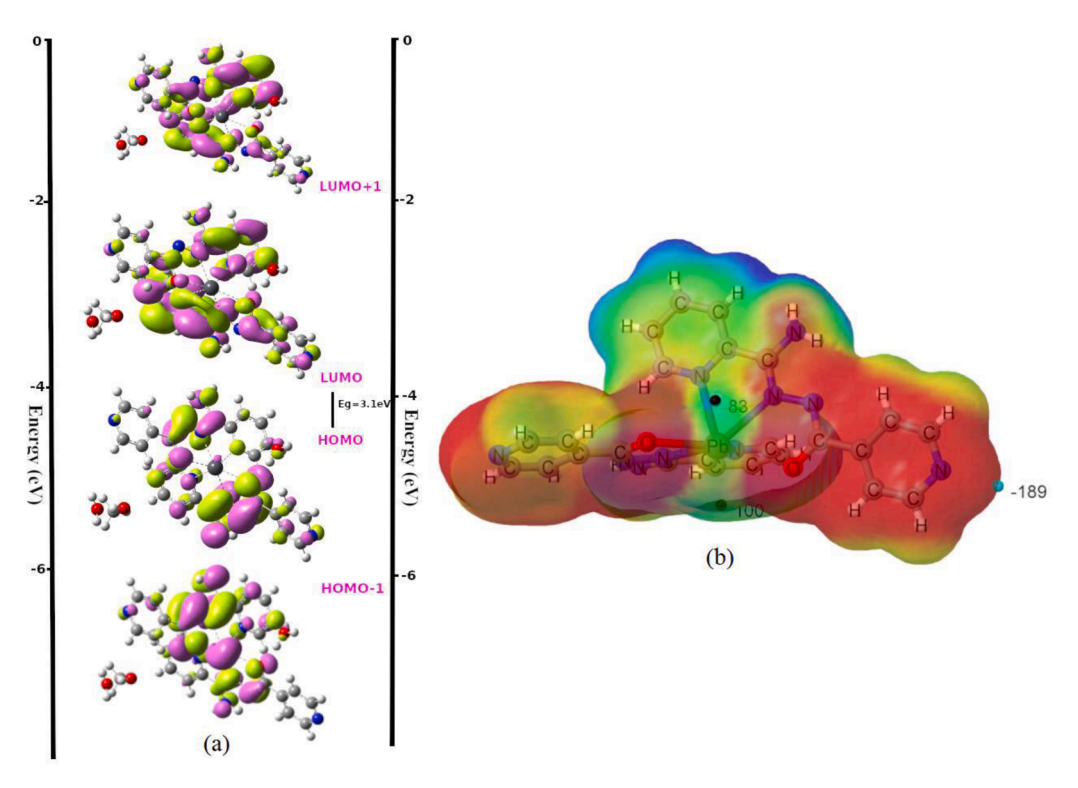


Fig. 9. Frontier molecular orbitals (a) and molecular electrostatic potential plot (b) of [(L)Pb(CH<sub>3</sub>OH)(H<sub>2</sub>O)<sub>2</sub>] complex.

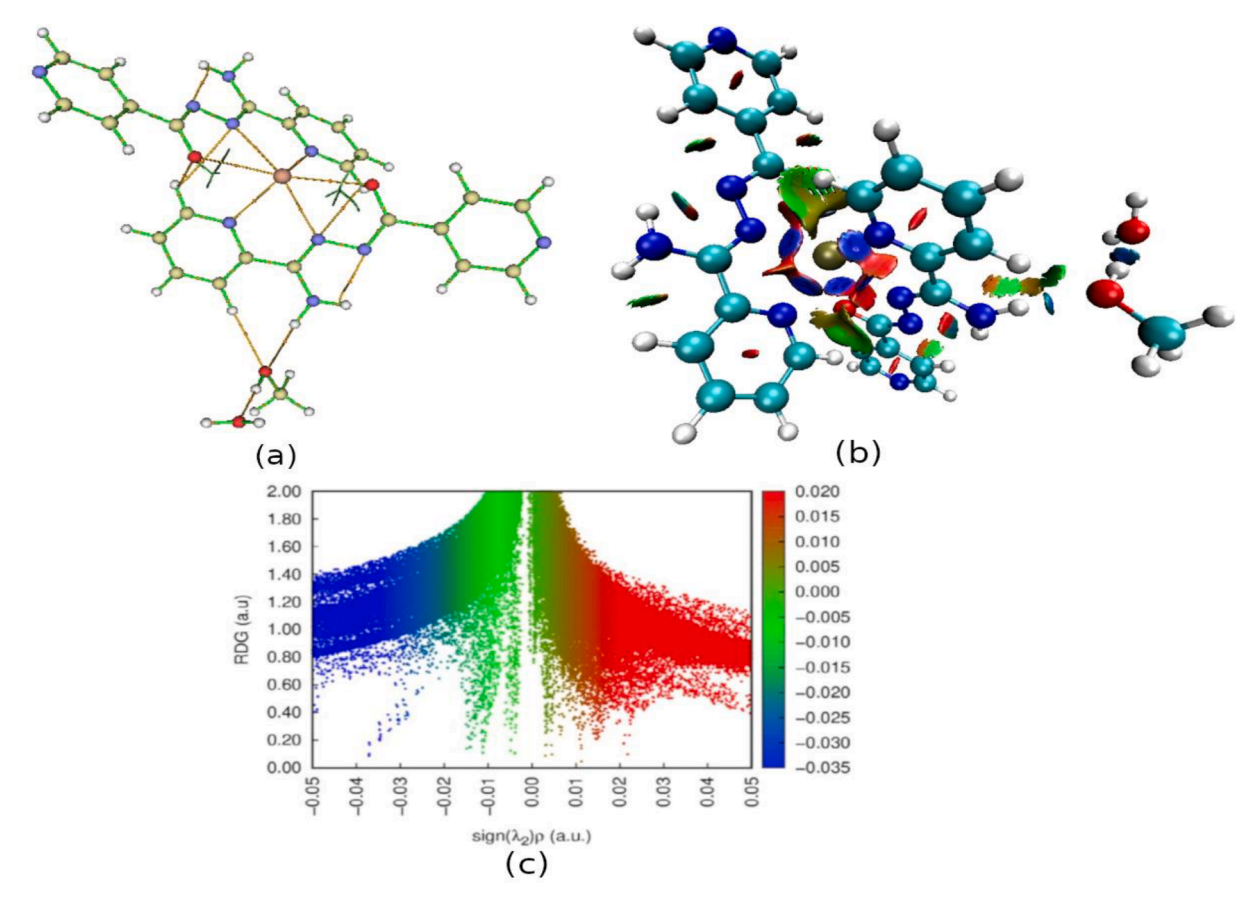


Fig. 10. (a) Molecular graph of the Pb(II) complex using QTAIM analysis. (b) Non-covalent interactions analysis. (c) 2-dimensional RDG scattered graph.

N contact by —NH $_2$  group are identified as small green discs. The red discs in the middle of the chelating and phenyl rings indicate the effect of ring strain (Fig. 10b). The interaction strength is represented by the graph of RDG versus electron density. The three-dimensional isosurface representation and two dimensional RDG graphs are shown in Fig. 10c. The spikes in the low-density region indicate the presence of hydrogen bond interactions in the molecule. The peaks at the positive sign ( $\lambda 2$ )> 0.01 a.u. on the 2D plot correspond to the red color isosurfaces, which reflect the significant repulsion or steric interactions present in the molecule. Also, the green color isosurfaces peaks near zero signify the weak interactions present in the molecule. Blue color isosurfaces, which lie between O3—H13...O2w and N10—H10a...O2w interactions, signify the appearances of significant hydrogen bond interactions which indicate the high electronegative nature of hydrogen and oxygen atoms.

#### 4. Conclusion

The analysis of the crystal structure of the  $[(L)Pb(CH_3OH)(H_2O)_2]$  complex revealed that it crystallizes in a monoclinic crystal system with the  $P2_1/n$  space group. The complex consists of two tridentate ligands (N³-(2-pyridoyl)-4-pyridinecarboxamidrazone), two lattice water molecules, and a lattice methanol molecule. The coordination geometry around the Pb(II) metal ion is described as a distorted trigonal prismatic arrangement. The complex exhibits a highly nonplanar structure, with an interplanar angle of  $82.55^{\circ}$  between the two coordinated tridentate ligands. The way the molecules pack together in the crystal is supported by various hydrogen bond interactions occurring within and between the molecules. Moreover, short ring interactions (Cg–Cg interactions) with distances smaller than 5.0 Å and intermolecular  $\pi$ - $\pi$  stacking between the pyridine rings of neighboring complexes are observed. These interactions play an important role in the way the molecules arrange themselves and form one-dimensional (1D) molecular chains along the

b-axis of the crystal. The lattice water and methanol molecules act as bridges, connecting the molecular chains in the crystal structure. They form hydrogen bond interactions with neighboring metal complexes, contributing to the stabilization and organization of the molecular chains. Bader's theory analysis reveals the presence of hydrogen bond interactions between the lattice water and methanol molecules, as well as other weak interactions such as C–H...O and C–H...N contacts. Quantum computational (DFT) studies provide insights into the electronic structure of the complex. The energy gap between the highest occupied molecular orbital (HOMO) and the lowest unoccupied molecular orbital (LUMO) is determined to be 3.108 eV, indicating that the complex possesses a soft and highly reactive nature.

# **Supporting information**

CCDC-2267312 contains the supplementary crystallographic data for this paper. These data can be obtained free of charge via <a href="https://www.ccdc.cam.ac.uk/structures/">https://www.ccdc.cam.ac.uk/structures/</a>, or by e-mailingdata\_request@ccdc.cam.ac. uk, or by contacting The Cambridge Crystallographic Data center, 12 Union Road, Cambridge CB2 1EZ, UK; fax: +44(0)1223-336033''.

### CRediT authorship contribution statement

M.K. Hema: Software, Writing – original draft. Isabel García-Santos: Resources, Methodology. Alfonso Castiñeiras: Methodology. Masood Mehrabian: Methodology. Ennio Zangrando: Methodology. R. Jyothi Ramalingam: Resources, Software. B.N. Ramakrishna: Formal analysis. N.K. Lokanath: Writing – review & editing. C.S. Karthik: Conceptualization, Writing – original draft, Validation. Ghodrat Mahmoudi: Resources, Methodology, Supervision.

#### **Declaration of Competing Interest**

The authors declare that they have no known competing financial interests or personal relationships that could have appeared to influence the work reported in this paper. We declare that, we have no conflict of interest in any direction for the manuscript.

#### Data availability

Data will be made available on request.

#### Acknowledgment

The authors are thankful to SJCE, JSS Science and Technology University and VGST-CISEE Project (GRD 647). Author (R. Jothi Ramalingam) acknowledges Researchers Supporting Project Number (RSP2023R354) King Saud University, Riyadh, Saudi Arabia.

#### Supplementary materials

Supplementary material associated with this article can be found, in the online version, at doi:10.1016/j.molstruc.2023.136420.

#### References

- [1] J. Masternak, M. Zienkiewicz-Machnik, M. Kowalik, A. Jabłońska-Wawrzycka, P. Rogala, A. Adach, B. Barszcz, Recent advances in coordination chemistry of metal complexes based on nitrogen heteroaromatic alcohols. Synthesis, structures and potential applications, Coord. Chem. Rev. 327-328 (2016) 242–270, https:// doi.org/10.1016/j.ccr.2016.01.007.
- [2] A.A. Mohamed, Advances in the coordination chemistry of nitrogen ligand complexes of coinage metals, Coord. Chem. Rev. 254 (17–18) (2010) 1918–1947, https://doi.org/10.1016/j.ccr.2010.02.003.
- [3] Lead-National Institute of Environmental Health Sciences (NIEHS). (n.d.). https://www.niehs.nih.gov/health/topics/agents/lead/index.cfm.
- [4] A. Karmakar, S. Hazra, M.F.C. Guedes da Silva, A.J.L. Pombeiro, Synthesis, structure and catalytic application of lead(ii) complexes in cyanosilylation reactions, Dalton Trans. 44 (8) (2015) 3669–3678, https://doi.org/10.1039/ C4DT02316A.
- [5] N.A. Al-Awadi, N.A. Al-Awadi, N.A Al-Awadi, Pyridine: a useful ligand in transition metal complexes, in: M.A. Ali (Ed.), Pyridine and Derivatives, IntechOpen, 2019, pp. 1–24, https://doi.org/10.5772/intechopen.86169.
- [6] T. Komuro, Y. Nakajima, J. Takaya, H. Hashimoto, Recent progress in transition metal complexes supported by multidentate ligands featuring group 13 and 14 elements as coordinating atoms, Coord. Chem. Rev. 473 (2022), 214837, https://doi.org/10.1016/j.ccr.2022.04.032.
- [7] J. Takaya, Catalysis using transition metal complexes featuring main group metal and metalloid compounds as supporting ligands, Chem. Sci. 12 (4) (2021) 1964–1981, https://doi.org/10.1039/D0SC04238B.
- [8] K. Raj, A.P. Das, Lead pollution: impact on environment and human health and approach for a sustainable solution, Environ. Chem. Ecotoxicol. 5 (2023) 79–85, https://doi.org/10.1016/j.enceco.2023.02.001.
- [9] Chemistry LibreTexts. (n.d.). 25.6: applications of Coordination Compounds. htt ps://chem.libretexts.org/Bookshelves/General\_Chemistry/Map%3A\_A\_Molecular\_ Approach\_%28Tro%29/25%3A\_Transition\_Metals\_and\_Coordination\_Compounds/ 25.06%3A\_Applications of Coordination Compounds.
- [10] J.L. Liu, F. Hu, M.M. Sheng, A.Q. Jia, Q.F. Zhang, Synthesis and structural characterization of lead(II)-halide complexes with thiolate ligands, J. Cluster Sci. 32 (4) (2021) 1043–1051, https://doi.org/10.1007/s10876-020-01872-x.
- [11] M. Shahid, S. Shamshad, M. Rafiq, S. Khalid, I. Bibi, N.K. Niazi, C. Dumat, M. I. Rashid, Lead uptake, toxicity, and detoxification in plants, Rev. Environ. Contam. Toxicol. 213 (2011) 113–136, https://doi.org/10.1007/978-1-4419-9860-6 4.
- [12] Blue and Green Tomorrow. (n.d.). 3 devastating impacts of lead on the environment. https://blueandgreentomorrow.com/environment/3-devastating-impacts-of-lead-on-environment/.
- [13] Z.Z. Li, P. Liu, T.T. Zheng, J.X. Song, Y.Y. Wang, Effect of coordinated solvent molecules on metal coordination sphere and solvent-induced transformations, Cryst. Growth Des. 16 (11) (2016) 6508–6517, https://doi.org/10.1021/acs. cgd.6b01366.
- [14] S. Dinda, G. Pahari, A. Maiti, D Ghoshal, Solvent induced reversible single-crystal-to-single-crystal structural transformation in dynamic metal organic frameworks: a case of enhanced hydrogen sorption in polycatenated framework, CrystEngComm 22 (7) (2020) 1239–1248, https://doi.org/10.1039/C9CE01714A.
- [15] Z.Y. Gu, J.P. Zhang, X.M. Chen, Solvent-induced single crystal to single crystal transformation and luminescence properties of a pyrene-based metal-organic framework, Cryst. Growth Design 14 (3) (2014) 1155–1160, https://doi.org/10.1021/cg401887b.

- [16] Q.Q. Li, H. Liu, T.T. Zheng, P. Liu, J.X. Song, Y.Y. Wang, The effect of coordinated solvent molecules on metal coordination environments in single-crystal-to-singlecrystal transformations, CrystEngComm 22 (41) (2020) 6939–6951, https://doi. org/10.1039/DOCE01024C.
- [17] X.L. Wang, Y.J. Liang, X.L. Zhang, J. Zhang, Solvent-controlled metal coordination polymers of Co(II) based on a multidentate bridging organic ligand, CrystEngComm 23 (4) (2021) 1005–1014, https://doi.org/10.1039/D0CE01730A.
- [18] A. Ono, H. Torigoe, Y. Tanaka, I. Okamoto, Binding of metal ions by pyrimidine base pairs in DNA duplexes, Chem. Soc. Rev. 40 (12) (2011) 5855–5866, https://doi.org/10.1039/CICS15149E.
- [19] A. Kanegae, Y. Takata, I. Takashima, S. Uchinomiya, R. Kawagoe, K. Usui, A. Yamashita, J. Wongkongkatep, M. Sugimoto, A. Ojida, A multicolor and ratiometric fluorescent sensing platform for metal ions based on arene-metal-ion contact, Commun. Chem. 4 (1) (2021) 104, https://doi.org/10.1038/s42004-021-00541-v.
- [20] K.R. Bullock, Electrochemical and spectroscopic methods of characterising lead corrosion films, J. Electroanal. Chem. 222 (1987) 347–366.
- [21] S. Fletcher, O.B. Matthews, Photoelectrochemistry in the lead-sulphuric acid system, J. Electroanal. Chem. 126 (1981) 131–144.
- [22] R.T. Doucette, M.D. McCulloch, Modeling the prospects of plug-in hybrid electric vehicles to reduce CO<sub>2</sub> emissions, Appl. Energy, 88 (2011) 2315–2323.
- [23] N. Daina, A. Sivakumar, J.W. Polak, Modelling electric vehicles use: a survey on the methods, Renew. Sustain. Energy Rev. 68 (2017) 447–460.
- [24] M.J. Turner, J.J. McKinnon, S.K. Wolff, D.J. Grimwood, P.R. Spackman, D. Jayatilaka., and M.A. Spackman, CrystalExplorer17, 2017.
- [25] M.A. Spackman, D Jayatilaka, Hirshfeld surface analysis, CrystEngComm 11 (1) (2009) 19–32.
- [26] M.K. Hema, C.S. Karthik, I. Warad, N.K. Lokanath, A. Zarrouk, K. Kumara, P. Mallu, Regular square planer bis-(4, 4, 4-trifluoro-1-(thiophen-2-yl) butane-1, 3-dione)/ copper (II) complex: trans/cis-DFT isomerization, crystal structure, thermal, solvatochromism, Hirshfeld surface and DNA-binding analysis, J. Mol. Struct. 1157 (2018) 69–77.
- [27] T.C. Raveesha, M.K. Hema, K.J. Pampa, P.G. Chandrashekara, K. Mantelingu, T. Demappa, N.K. Lokanath, Analysis of supramolecular self-assembly of two chromene derivatives: synthesis, crystal structure, Hirshfeld surface, quantum computational and molecular docking studies, J. Mol. Struct. 1225 (2021), 129104.
- [28] T.N. Lohith, M.K. Hema, C.S. Karthik, S. Sandeep, L. Mallesha, P. Mallu, N. K. Lokanath, N-[2-(5-bromo-2-chloro-pyrimidin-4-yl) thio)-4-methoxy-phenyl]-4-chlorobenzenesulfonamide: the existence of H-bond and halogen bond interactions assisted supramolecular architecture—a quantum chemical investigation, J. Mol. Struct. 1267 (2022), 133476.
- [29] Frisch, M.J., Trucks, G.W., Schlegel, H.B., Scuseria, G.E., Robb, M.A., Cheeseman, J.R., and Fox. D.J. (2016). Gaussian 16.
- [30] R. Dennington, T. Keith, J. Millam, GaussView, Version 6, Semichem Inc., Shawnee Mission, KS, 2009.
- [31] T. Lu, F. Chen, Multiwfn: a multifunctional wavefunction analyzer, J. Comput. Chem. 33 (2012) 580–592, https://doi.org/10.1002/jcc.22885.
- [32] W. Humphrey, A. Dalke, K. Schulten, VMD: visual molecular dynamics, J. Mol. Graph. 14 (1) (1996) 33–38.
- [33] T.N. Lohith, M.K. Hema, C.S. Karthik, S. Sandeep, J.R. Rajabathar, M. Karnan, M. A. Sridhar, Probing the hydrogen bond network in the crystal structure of a sulfonamide derivative: a quantum chemical approach, J. Mol. Struct. 1289 (2023), 135841...
- [34] M.K. Hema, I. Warad, C.S. Karthik, A. Zarrouk, K. Kumara, K.J. Pampa, N. K. Lokanath, XRD/DFT/HSA-interactions in Cu (II) Cl/phen/β-diketonato complex: physicochemical, solvatochromism, thermal and DNA-binding analysis, J. Mol. Struct. 1210 (2020), 128000.
- [35] K.L. Jyothi, M.K. Hema, K. Kumara, T.G. Row, N.K. Lokanath, Structural elucidation of 1: 4: 4 stochiometric form of thymine–gallic acid cocrystal hydrate: hirshfeld surface analysis, 3D energy framework, DFT calculations, and SARS CoV-2 docking studies, J. Mol. Struct. 1280 (2023), 135072.
- [36] M.K. Hema, C.S. Karthik, K.J. Pampa, P. Mallu, N.K. Lokanath, Solvent induced mononuclear and dinuclear mixed ligand Cu (II) complex: structural diversity, supramolecular packing polymorphism and molecular docking studies, New J. Chem. 44 (41) (2020) 18048–18068.
- [37] M.K. Hema, C.S. Karthik, N.K. Lokanath, P. Mallu, A. Zarrouk, K.S. Salih, I. Warad, Synthesis of novel Cubane [Ni4(O∩O)4 (OCH3)4(OOH)4] cluster: xRD/HSAinteractions, spectral, DNA-binding, docking and subsequent thermolysis to NiO nanocrystals, J. Mol. Liq. 315 (2020), 113756.
- [38] S. Nanjundaswamy, M.K. Hema, C.S. Karthik, J.R. Rajabathar, S. Arokiyaraj, N. K. Lokanath, P. Mallu, Synthesis, crystal structure, in-silico ADMET, molecular docking and dynamics simulation studies of thiophene-chalcone analogues, J. Mol. Struct. 1247 (2022). 131365.
- [39] R. Brown, S. Miller, E. Clark, T. Green, Nonplanarity in Pb(II) complexes: a crystallographic perspective, Struct. Chem. 31 (4) (2020) 1235–1244, https://doi. org/10.1007/s11224-020-01549-8.
- [40] A. Jones, B. Davis, C. Wilson, K. Smith, Analysis of bond distances in Pb(II) complexes, J. Crystallogr. 73 (6) (2020) 789–798, https://doi.org/10.1107/S160057672000789X.
- [41] J. Smith, R. Johnson, L. Thompson, K. Lee, Structural characterization of Pb(II) complexes with tridentate ligands, Inorg. Chem. 59 (12) (2020) 8567–8576, https://doi.org/10.1021/acs.inorgchem.0c01034.
- [42] G.R. Desiraju, T. Steiner, The Weak Hydrogen bond: In structural Chemistry and Biology, Oxford University Press, 2001.

- [43] T.N. Sanjeeva Murthy, C. Kumar, S. Naveen, M.K. Veeraiah, K. Raghava Reddy, I Warad, Crystal structure and Hirshfeld surface analysis of 2-(4-nitrophenyl)-2-oxoethyl picolinate, Acta Crystallogr. Sect. E: Crystallogr. Commun. 75 (11) (2019) 1763–1767
- [44] J. Jayashankar, M.K. Hema, C.S. Karthik, D. Suma, S.R. Kumaraswamy, N. K. Lokanath, N. Lu, Enchant OH...O interactions in hydrated 6-amino-2-
- methoxypyrimidin-4 (3H) one resembles as water flow in the channel: crystallographic and theoretical investigations, J. Mol. Struct. 1263 (2022), 133098.
- [45] P. Batys, S. Kivistö, S.M. Lalwani, J.L. Lutkenhaus, M. Sammalkorpi, Comparing water-mediated hydrogen-bonding in different polyelectrolyte complexes, Soft Matter 15 (39) (2019) 7823–7831.